

# An Experiment of the Malkus-Lorenz Waterwheel and Its Measurement by Image Processing

Heewon Kim

*Department of mathematics, Ewha womans university, Seoul, Korea, 03762*

Jiwon Seo

*Department of mathematics, Ewha womans university, Seoul, Korea, 03762*

Bora Jeong

*Department of mathematics, Ewha womans university, Seoul, Korea, 03762*

Chohong Min<sup>\*</sup>

*Department of mathematics, Ewha womans university, Seoul, Korea, 03762*

Received (to be inserted by publisher)

We introduce a simple and efficient experiment setup for the Malkus-Lorenz waterwheel. Through a series of image processing techniques, our work is listed as one of the few experiments that measure not only the angular velocity but also the mass distribution. Our experiment is to observe qualitative changes on the waterwheel as the leakage rate changes, while the other physical parameters are fixed. We perform a bifurcation analysis for the qualitative changes, and the phase portraits from experiments are validated by the bifurcation analysis.

*Keywords:* Malkus-Lorenz waterwheel; bifurcation analysis; image processing; chaos

## 1. Introduction

Chaos has been a hot study topic that arises from natural phenomena such as leaky faucets, pendula, chemical reactions and lasers [Strogatz, 2008; Illing *et al.*, 2012]. These days, enormous data are created and spent by an increasing number of sources from social media to digital sensors in industrial machinery. Big data analysts try to explain the enormous and chaotic data and find an order out of the chaos [LaPlante, 2014]. Hence the demand to understand chaos in natural and social phenomena has grown much these days.

Being a typical example of chaotic dynamical systems, the Lorenz equations display many prototypical characteristics such as fractals, homoclinic explosion, and period-doubling cascade [Guckenheimer & Holmes, 1983]. Thus, understanding the Lorenz equations helps students and researchers to analyze chaotic dynamics in natural and social phenomena. Among many physical models explained by the equations, the chaotic waterwheel, which is first invented by Malkus [Malkus, 1972] in 1972, is the best known one. The motion of the waterwheel can be exactly described by the Lorenz equations, and gives an intuitive understanding of the equations.

---

<sup>\*</sup>corresponding author, chohong@ewha.ac.kr

Accurate construction of the waterwheel involves many nontrivial tasks, such as making leakage rate proportional to mass distribution. Tongen et al. [Tongen *et al.*, 2012] introduced a sandwheel which has constant leakage rate. Though achieving the constant leakage rate, they faced difficulties in making accurate measurements. Therefore, they focused only on mathematical analysis without physical construction. Their numerical analysis verify that bifurcation diagrams for sandwheel show large differences with Lorenzian dynamics bifurcation.

Also, Matson [Matson, 2007] as well as Kolar [Kolar & G.Gumbs, 1992] analyzed the behavior of the Malkus-Lorenz waterwheel and the roles of parameters that matches with the Lorenz parameters. They numerically analyze bifurcations from waterwheel parameters, without actual experiments. Visually identifying the result gives intuitive understanding to students. For that reason, doing actual experiment is important. Our paper suggests a simple construction for experiment, so following our experiment will bring students intuitions a lot.

To construct physical model which gives accurate results, some articles introduced the designs of waterwheel using special materials. Illing et al. [Illing *et al.*, 2012] suggested a very accurate construction of the waterwheel, whose dynamics is precisely described by the Lorenz equations. To achieve the fine accuracy, they also employed many special devices such as magnetic brake, rotational encoder, and rare earth magnets, which are hardly accessible to students.

R. Nemirovsky [Nemirovsky, 1993] aimed to bring students intuitions through actual experiment. They worked with kinetic sculpture, and employed special materials such as optical readout disk and oil viscometer for constructing waterwheel. It is difficult for students to construct waterwheel by themselves.

In overall, most articles about chaotic wheel are focused on numerical analysis without actual experiment, or special materials were used. In this article, our goal is to construct a waterwheel that can be built in a simple and easy way, and gives reasonably accurate results. Our construction requires only accessible materials in common stationery shops, and its dynamical behavior matches well with the bifurcation analysis of the Lorenzian equations. Our construction of the waterwheel is simple because we take the leakage rate as a variable, and the rate can be easily modified by the hole size punctured in the cups. Our experiment setup follows a well-known simple setting that is briefly reviewed in section 2. Most experiments so far report only the angular velocity [Mishra & Sanghi, 2006; Cho & Miyano, 2014; Matson, 2007]. Only few of them [Yang & Lin, 1998] report on the mass distribution from which the other two state variables are calculated. Though our experiment setup is simple, we built it with transparent acrylic and dyed water blue, which enabled us to measure the mass distribution efficiently. Section 4 introduces a series of novel and efficient image processing techniques for the measurement. In section 5, the experiment results collected through the image processing are compared to the bifurcation analysis performed in section 2. We leave in section 6 concluding remarks that evaluate the experiment setup, the measurement through image processing, and the comparison between the measurement and the bifurcation analysis.

## 2. Malkus-Lorenz Waterwheel

The Malkus-Lorenz waterwheel is a well-known physical implementation of the Lorenz equation. We briefly review the mathematical modeling of the waterwheel. The details can be found in [Kolar & Gumbs, 1992; Yang & Lin, 1998]. The waterwheel is a freely turning wheel to whose rims are attached several leaking cups. Figure 1 depicts an illustration and our actual construction of the wheel.

Being rigid, the rotation of the wheel is measured by its angular velocity  $\omega(t) \in \mathbb{R}$ . The amount of water in the cup at angle  $\theta \in [0, 2\pi)$  and time  $t$  is denoted by  $m(\theta, t)$ . The angular velocity and the mass distribution evolve with time according to the following conservation of mass and angular momentum.

$$\begin{aligned} \frac{\partial m(\theta, t)}{\partial t} + \omega(t) \frac{\partial m(\theta, t)}{\partial \theta} &= -K \cdot m(\theta, t) + Q(\theta) \\ \frac{d}{dt}[I \cdot \omega(t)] &= g \cdot r \int_0^{2\pi} m(\theta, t) \sin \theta d\theta - \nu \cdot \omega(t) \end{aligned} \quad (1)$$

Here  $Q(\theta)$  is the water inflow at angle  $\theta$ ,  $K$  is the leakage rate of the cups, and  $\nu$  is the damping rate in the rotation of the wheel. Being  $2\pi$ -periodic,  $Q(\theta)$  and  $m(\theta, t)$  can be expanded into the Fourier series. Because of the symmetry,  $Q(\theta)$  is an even function and is expanded by the cosine series as follows.

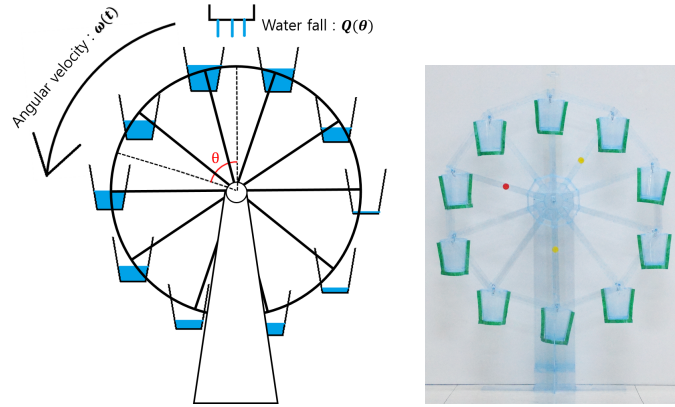


Fig. 1. Our experimental implementation

$$\begin{aligned} m(\theta, t) &= \sum_{n=0}^{\infty} [a_n(t) \sin n\theta + b_n(t) \cos n\theta] \\ Q(\theta) &= \sum_{n=0}^{\infty} q_n \cos n\theta \end{aligned} \quad (2)$$

The substitutions of  $m(\theta, t)$  and  $Q(\theta)$  in the conservation laws with the series expansions give rise to the following ordinary differential equations. Note that other Fourier coefficients are subsidiary to the first coefficients [Strogatz, 2008](page 341), and we concentrate only on the first coefficients.

$$\begin{aligned} a_1' &= -K a_1 + \omega b_1 \\ b_1' &= -\omega a_1 - K b_1 + q_1 \\ \omega' &= \frac{\pi g r}{I} a_1 - \frac{\nu}{I} \omega \end{aligned} \quad (3)$$

The ordinary differential equations can be transformed into the Lorenz equations by some non-dimensionalizations [Illing *et al.*, 2012] such as  $\sigma = \frac{\nu}{KI}$ ,  $\rho = \frac{q_1 g r \pi}{K^2 \nu}$ , and  $t^* = Kt + \frac{q_1}{K}$ .

$$\begin{aligned} x' &= \sigma(y - x) \\ y' &= \rho x - y - xz \\ z' &= xy - \beta z \end{aligned} \quad (4)$$

## 2.1. Bifurcation Analysis with respect to $K$

It has been a standard to study the qualitative change in the Lorenz equations when the parameter  $\rho$  gradually changes while the other parameters are fixed. However, it is not a simple task to implement the parameter change in the waterwheel experiment. Each physical parameter such as leakage rate  $K$  and damping rate  $\nu$  affects all the parameters  $\sigma = \frac{\nu}{KI}$  and  $\rho = \frac{q_1 g r \pi}{K^2 \nu}$  in the Lorenz equations. Thus the implementation of the standard study involves complex and complicated physical tune-ups.

Instead of the conventional study, we consider the variation of a physical parameter  $K$ , the leakage rate of the hanging cups, while the other physical parameters are fixed. The leakage rate is one of the easiest parameters to vary. Changing the radius of the leakage hole suffices to vary it.

Fixed points are where all the time derivatives vanish. A simple calculation that solves  $a_1' = b_1' = \omega' = 0$  in equation (3) gives the fact that there are only the following three fixed points in the system.

$$\begin{aligned} C_0 &= (0, \frac{q_1}{K}, 0), \text{ and} \\ C_{\pm} &= \left( \pm \frac{\nu}{\pi g r} \sqrt{K_p^2 - K^2} \right) \text{ if } K \leq K_p, \text{ where } K_p := \sqrt{\frac{q_1 \pi g r}{\nu}}. \end{aligned}$$

According to the Hartman-Grobman theorem [Perko, 2001], the nonlinear system (3) around the fixed points have the same qualitative features as its linearized system as long as the fixed points are hyperbolic. We therefore look into the Jacobian matrices of the nonlinear system at the fixed points.

The characteristic polynomial of each Jacobian matrix is listed below.

$$C_0 : (x + K) \left( x^2 + \left( K + \frac{\nu}{I} \right) x + \frac{K\nu}{I} - \frac{q_1 \pi g r}{K_i} \right) = 0$$

$$C_{\pm} : x^3 + \left( 2K + \frac{\nu}{I} \right) x + \left( \frac{K\nu}{I} + \frac{q_1 \pi g r}{\nu} \right) x + \frac{q_1 \pi g r}{I} - \frac{\nu K^2}{I} = 0$$

The stability of each fixed point can be easily examined by the Routh-Hurwitz criteria [Strikwerda, 1989]. A fixed point is hyperbolic and stable, if the characteristic polynomial of the Jacobian matrix at the fixed point is Hurwitz, i.e., having all the roots in the left half-plane  $\{z \in \mathbb{C} | \text{Re}(z) < 0\}$ . A cubic polynomial  $x^3 + c_2 x^2 + c_1 x + c_0$  is Hurwitz if and only if  $c_2 c_0 > 0$  and  $c_2 c_1 > c_0$  [Strikwerda, 1989]. The application of the criteria to each of the fixed points makes the following results.

$$C_0 \text{ is stable only when } K \in (K_P, \infty), \text{ and}$$

$$C_{\pm} \text{ are stable only when } K \in (K_H, K_P),$$

$$\text{where } K_H := \frac{-(2q_1 \pi g r I^2 + \nu^3) + \sqrt{(2q_1 \pi g r I^2 + \nu^3)^2 + 16\nu^3 I^2 q_1 \pi g r}}{8\nu^2 I}$$

The results indicate that the pitchfork bifurcation occurs at  $K = K_P$ . When  $K = K_H$ , the equality  $c_2 c_1 = c_0$  holds, and the cubic polynomial has two imaginary roots  $\pm i\sqrt{c_1}$ , which suggests the occurrence of the Hopf bifurcation [Perko, 2001].

From the numerical results in figure 2 and the criteria of Hopf bifurcation in [Strogatz, 2008] (page 252), we may conclude that the Hopf bifurcation is subcritical. The bifurcation analysis is illustrated in figure 3. The physical parameters taken in our experiment setup are listed below. An estimation of the parameters and the other details are discussed in section 3.

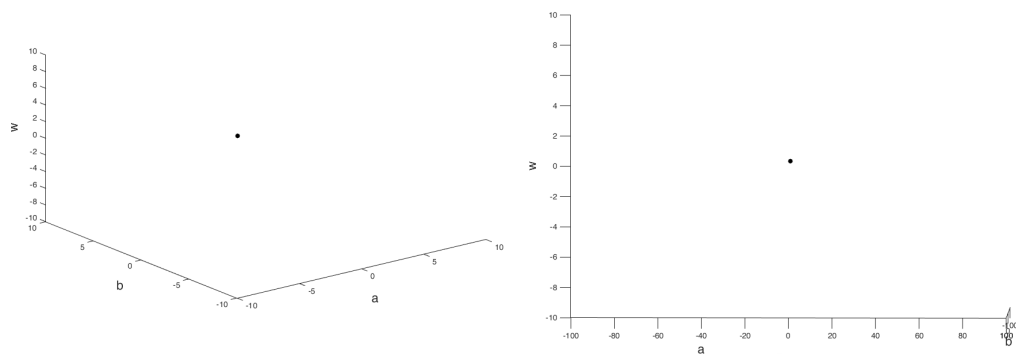
parameter	value
moment of inertia ( $I$ )	232000 $g \cdot \text{cm}^2$
damping rate ( $\nu$ )	52700 $g \cdot \text{cm}^2/s$
water inflow rate ( $q_1$ )	17.7 $g/s$
radius ( $r$ )	26.0 $\text{cm}$
leakage rate ( $K$ )	variable

### 3. Experiment Setup

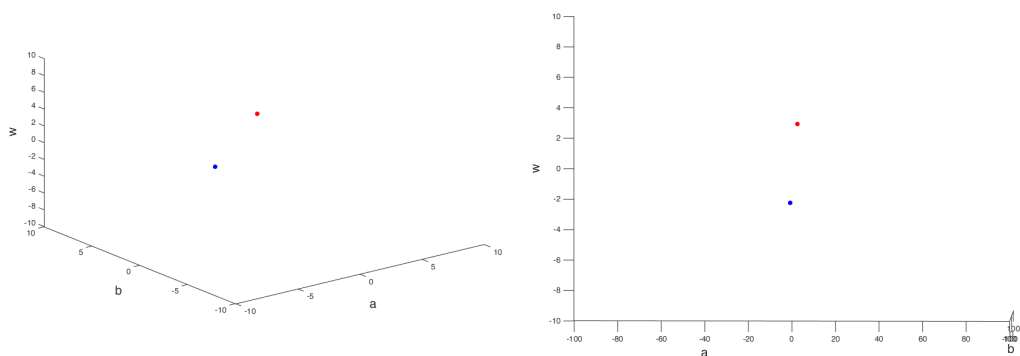
We take a conventional setup for constructing the waterwheel. As illustrated in figure 1, ten leaky cups are simply hanging on the rims of the wheel. The setup is not accurate to the mathematical model in section 2 in several aspects. Because of the existing gaps between cups, water inflow sometimes does not add up. Water leaked out from the cups in the top may flow into the cups in the bottom. A better setup locates the wheel not vertically but with some slanted angle [Illing *et al.*, 2012; Matson, 2007]. The setup resolves the two defects. To properly implement the assumption that the leakage rate is constant, a long thin leakage pipe needs be appended to each cup [Illing *et al.*, 2012].

Our aim is to measure not only the angular velocity but also the mass distribution. In the conventional setting in figure 1, all the cups face the front. A camera in the front records the wheel with water colored with ink. We suggest an image processing algorithm that analyzes the captured images and measures the mass distribution from locating colored regions.

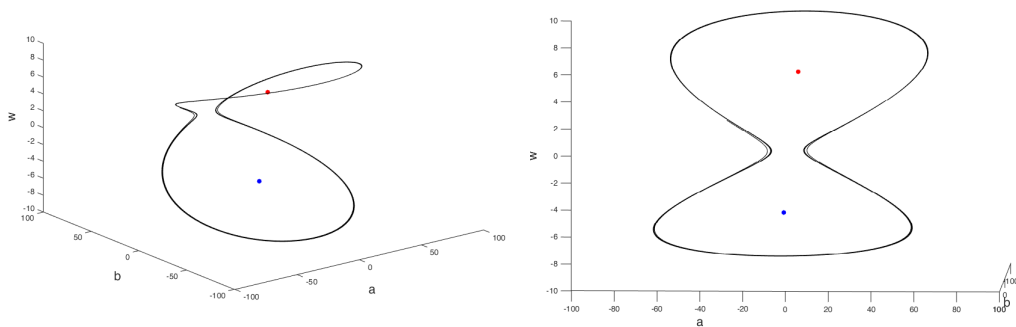
The stand and the wheel were constructed from sheets of transparent acrylic, which was bought cheap at a nearby stationery store. Between the ends of the stand, an axle of Acrylic tube was connected. Around the axle, another axle of iron tube was wrapped up and connected to the wheel. Thus the damping rate of the rotation is determined by the friction between the two co-annular axles, The combination of the iron and acrylic axles turn out to allow very smooth rotation. The details of the construction are illustrated in figure 4.



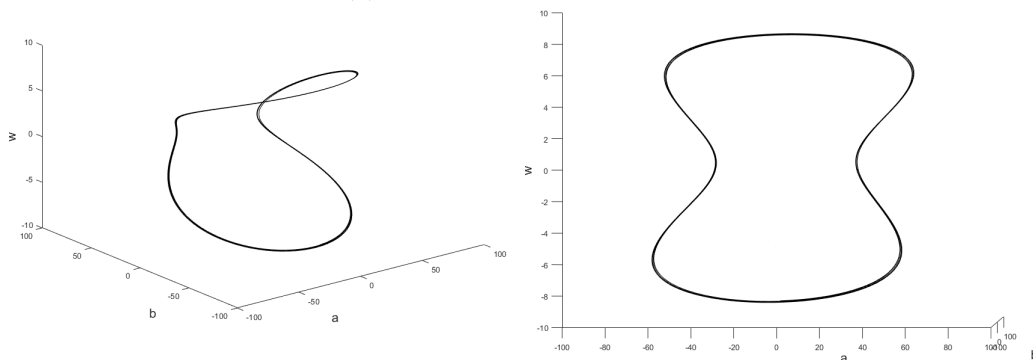
(a)  $K > K_p, K = 6.0$



(b)  $K_S < K < K_P, K = 4.5$



(c)  $K_H < K < K_S, K = 1.5$



(d)  $0 < K < K_H, K = 0.05$

Fig. 2. Fixed points and periodic orbits for chosen parameters  $K = 6.0, 4.5, 0.15$  and  $0.05$ .

### 3.1. Moment of Inertia

To calculate the moment of inertia, we use the physical formulas for typical solid shapes. Each spoke is a long thin stick whose end is attached to the axis of rotation, and its inertia value is  $\frac{1}{3}ml^2$ , where  $m$  is

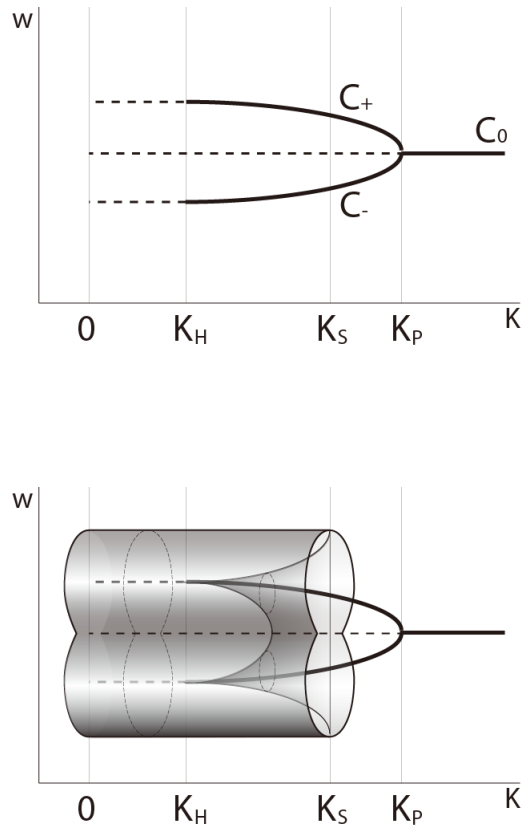


Fig. 3. Bifurcation diagrams of the fixed points (top) and the fixed points together with limit cycles (bottom).

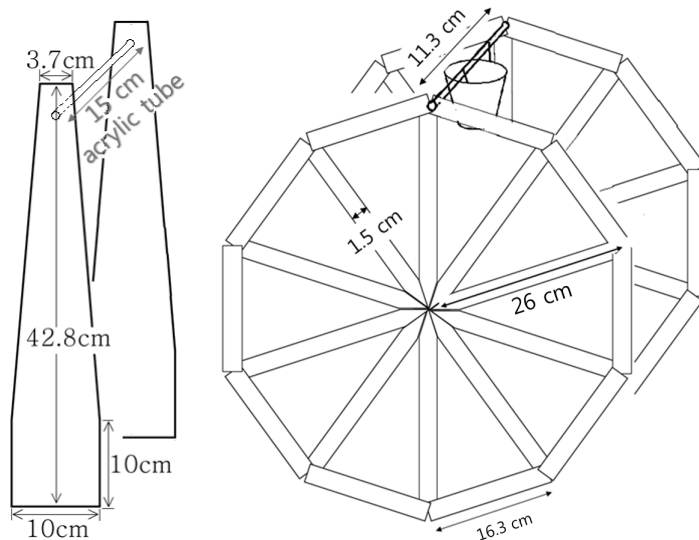


Fig. 4. Experiment setup

its mass and  $l$  is its length. Each stick, forming an arc of the wheel, has approximate inertia value  $ml^2$ . Summing up the inertia values of all the components of the waterwheel, we have the total moment of

inertia  $I = 2.33 \times 10^5 g \text{ cm}^2$ .

### 3.2. Damping Rate

To determine the damping rate  $\nu$  in equation (3), we spun the wheel without water inflow. The angular speed is slowed down due to the damping, accordingly to  $I\omega' = -\nu\omega$ . The angular speed exponential decreases to zero as  $\omega(t) = \omega_0 e^{-\frac{\nu}{I}t}$  and the angle  $\theta(t)$ , which is its anti-derivative, approaches a constant value  $\theta_\infty$ , as  $\theta(t) = \theta_\infty - \frac{I}{\nu}\omega_0 e^{-\frac{\nu}{I}t}$ . We recorded the spinning by a camera and measured the angle by the position of a red marker on the rim. The recorded video was spanned into a series of images, each of which was analyzed to position the marker by an image processor that we programmed. The C++ code of the processor is attached in the appendix. The parameter  $\nu$  was determined by fitting the measurement data by the formula as in figure 5.

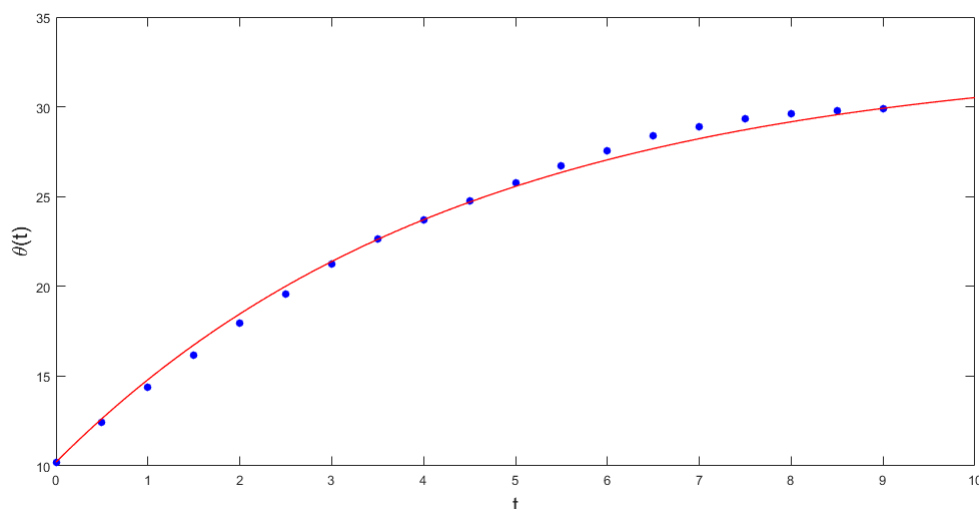


Fig. 5. After a free spinning, the angle  $\theta(t)$  was measured and marked as dots in the graph. Fitting the dots by the formula  $\theta(t) = \theta_\infty - \frac{I}{\nu}\omega_0 e^{-\frac{\nu}{I}t}$ , the damping rate  $\nu = 5.27 \times 10^4 g \cdot \text{cm}^2/s$  was calculated.

### 3.3. Leakage Rate

The bottom of each cup was punctured at the center. Initially filling the cup with 100ml water, we measured the time taken to spill each 10ml. The mass in the cup is assumed to satisfy  $m' = -Km$ , whose solution is  $m(t) = 100e^{-Kt}$ . As shown in figure 6, the parameter  $K$  was determined by the formula  $100e^{-Kt}$ . In this way, five different hole sizes were tried, and their corresponding leakage rate is given below.

Hole area( $\text{cm}^2$ )	$K$ (leakage rate)
0.0225	0.0581
0.0306	0.0714
0.0400	0.0987
0.0625	0.1453
0.1806	0.4030

Table 3.3

### 3.4. Water Inflow Rate

Water was steadily poured from the top with flow rate  $55.6g/s$  through a hose with radius  $\tilde{r} = 0.45\text{cm}$ . Let  $r = 26\text{cm}$  be the radius of the wheel, then the inflow rate at each angle  $\theta$  is given by  $Q(\theta) =$

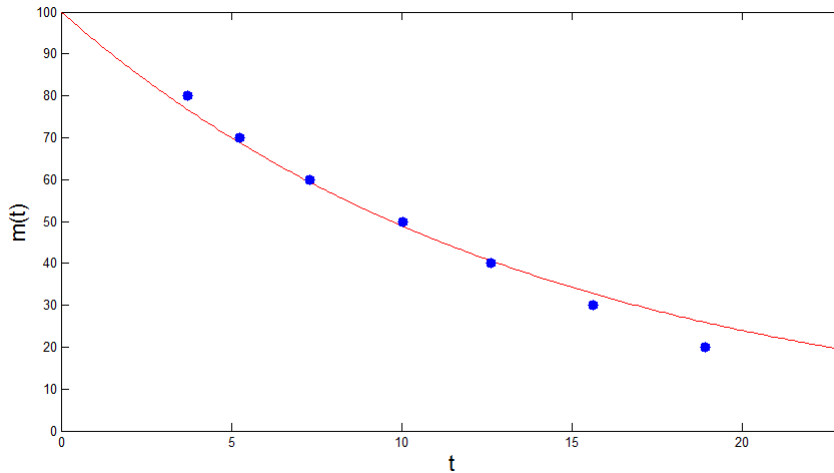


Fig. 6. The mass of a leaking cup was measured and marked as dots. The leakage rate  $K$  was calculated to be  $7.14 \times 10^{-2} \cdot g/s$  by fitting the dots by the formula  $m(t) = 100 \cdot e^{-Kt}$ .

$2r \cos \theta \sqrt{\tilde{r}^2 - (r \sin \theta)^2} \times \frac{55.6}{\pi \tilde{r}^2}$ . The Fourier coefficient  $q_1$  was calculated by the following integral.

$$q_1 = \frac{2}{\pi} \int_0^\pi Q(\theta) \cos \theta d\theta = 1.77 \times 10^1 g/s$$

#### 4. Measurement

To measure the angle of rotation  $\theta(t)$  and mass distribution  $m(\theta, t)$ , we introduce a series of image processing techniques that are carried out to each captured image of the waterwheel. The waterwheel is an articulated rigid body. The first degree of freedom is the rotation of the wheel around the axis, and there is another degree of freedom that each cup may rotate around the axis of its attachment to the rim. An image can be regarded as a function  $\vec{u} : \mathbb{R}^2 \rightarrow [0, 1]^2$ , where the domain  $\mathbb{R}^2$  includes the rectangular support of the domain and the codomain  $[0, 1]^3$  consists of the three principal colors: red, green, and blue.

To capture the rotation of the wheel, three dots are marked on the middle of the rims as in figure 7. One dot is colored in red, and the others in yellow. Initially the red dot is placed on the top. Let  $R(\theta)$  be the region of the red dot after the rotation by angle  $\theta$ , and  $Y_1(\theta)$  and  $Y_2(\theta)$  be those of the yellow dots. From the captured image  $\vec{u}$ , the rotation of the wheel from the initial position can be measured by solving the following optimization problem.

$$\text{Find } \theta \in [0, 2\pi] \text{ that minimizes } E_1(\theta),$$

$$\text{where } E_1(\theta) := \int_{R(\theta)} [\vec{u}(x) - (1, 0, 0)]^2 dx + \int_{Y_1(\theta) \cup Y_2(\theta)} [\vec{u}(x) - (1, 1, 0)]^2 dx.$$

When  $\theta$  matches the actual rotation, the color  $\vec{u}$  is red in  $R(\theta)$  and yellow in  $Y_1(\theta) \cup Y_2(\theta)$ , making  $E_1(\theta) = 0$ . There is no other place colored red except  $R(\theta)$  and no other place yellow except  $Y_1(\theta) \cup Y_2(\theta)$ . Therefore  $E_1(\theta) > 0$ , when  $\theta$  is inaccurate. Figure 7 shows that the minimization correctly locates the angle of rotation of the wheel.

The other degree of freedom is the rotation of each freely hanging cup. To detect the angle of the rotation, green marking tape is attached around the front section of each cup, as depicted in figure 8. Let  $P_i$  be the axis of rotation of the  $i$ th cup, and  $G(P_i, \theta)$  be the region of the green marker after the rotation by angle  $\theta$  around the axis  $P_i$ . The angle of the  $i$ th cup can be measured by solving the following optimization problem.

$$\text{Find } \theta_i \in [0, 2\pi] \text{ that minimizes } E_2(P_i, \theta_i),$$

$$\text{where } E_2(P_i, \theta_i) := \int_{G(P_i, \theta_i)} [\vec{u}(x) - (0, 1, 0)]^2 dx.$$

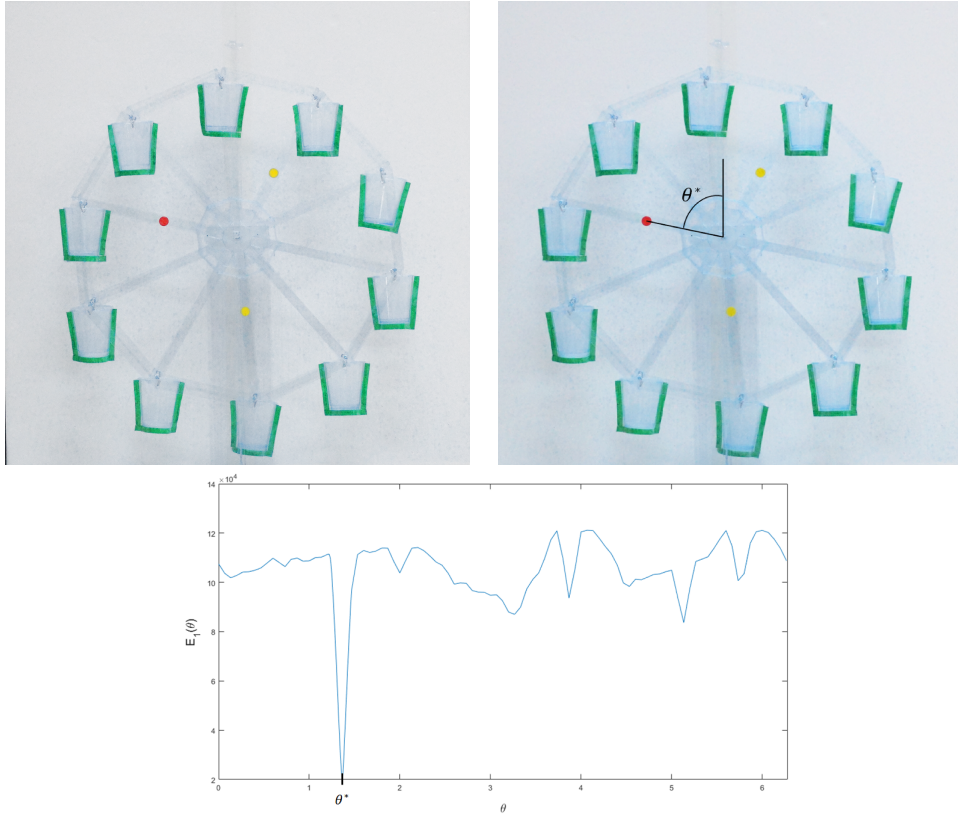


Fig. 7. A captured image  $\vec{u}$  (top left) and the minimization of  $E_1(\theta)$  by  $\theta = \theta^*$  (bottom). The minimum point  $\theta^*$  matches the actual rotation (top right).

Similarly to the minimization of  $E_1(\theta)$ , the value  $E_2$  becomes zero at the correct angle of rotation and positive elsewhere. Figure 8 shows the accurate identification of the angle through the minimization.

The functions  $E_1$  and  $E_2$  are not smooth with respect to the angle. The minimizations are solved by a brute-force way, selecting the angle with the smallest function value among 100 equally spaced samples in  $[0, 2\pi]$ . The angle, let us call  $\theta$ , is then refined by taking the smallest function value among another 100 equally spaced angles in  $[\theta - \frac{2\pi}{100}, \theta + \frac{2\pi}{100}]$ .

Once the position and rotation of each cup is estimated, the amount of water in each cup is approximated as follows. Let  $\Omega(P_i, \theta_i)$  be the region of the  $i^{\text{th}}$  cup with axis  $P_i$  and rotation  $\theta_i$ .

$$m(\theta, t) \simeq \sum_{\text{Pixel}(x,y) \in \Omega(P_i, \theta_i)} H(u(\vec{x}, y)) \cdot L((x, y), \Omega(P_i, \theta_i)) \cdot \Delta x \cdot \Delta y$$

Here  $H$  is the index function whose value is one when  $u(\vec{x}, y)$  has the dyed color and zero otherwise. The shape of the cup is a part of the cone. The pixel point  $(x, y)$  stands for a ray passing through the three dimensional cone.  $L((x, y), \Omega(P_i, \theta_i))$  denotes the length of the line segment of the ray inside the cone.

## 5. Experiment

In this section, our experiments of the waterwheel are reported. All the physical parameters except the leakage rate  $K$  are fixed by the constants given in table 3.3. According to the bifurcation analysis in section 2, there exist three important bifurcation values. When  $K$  is too large, the waterwheel stays motionless ( $C_0$ ) in the long run. At  $K = K_P \simeq 5.18$ , the pitchfork bifurcation occurs and the waterwheel rotates with constant angular velocity either clockwise ( $C_-$ ) or counter-clockwise ( $C_+$ ). At  $K = K_S \simeq 0.155$ , the saddle-node bifurcation generates one stable limit cycle and one unstable limit cycle. After quite a short time period,  $K$  reaches  $K_H \simeq 0.113$ . At  $K = K_H$  arises the subcritical Hopf-bifurcation that makes the unstable limit cycle collapse into  $C_{\pm}$ . After  $K = K_H$ , remains only the stable limit cycle. To validate the bifurcation analysis through experiments, we tried three  $K$  values. Two values are chosen from  $(0, K_H)$ ,

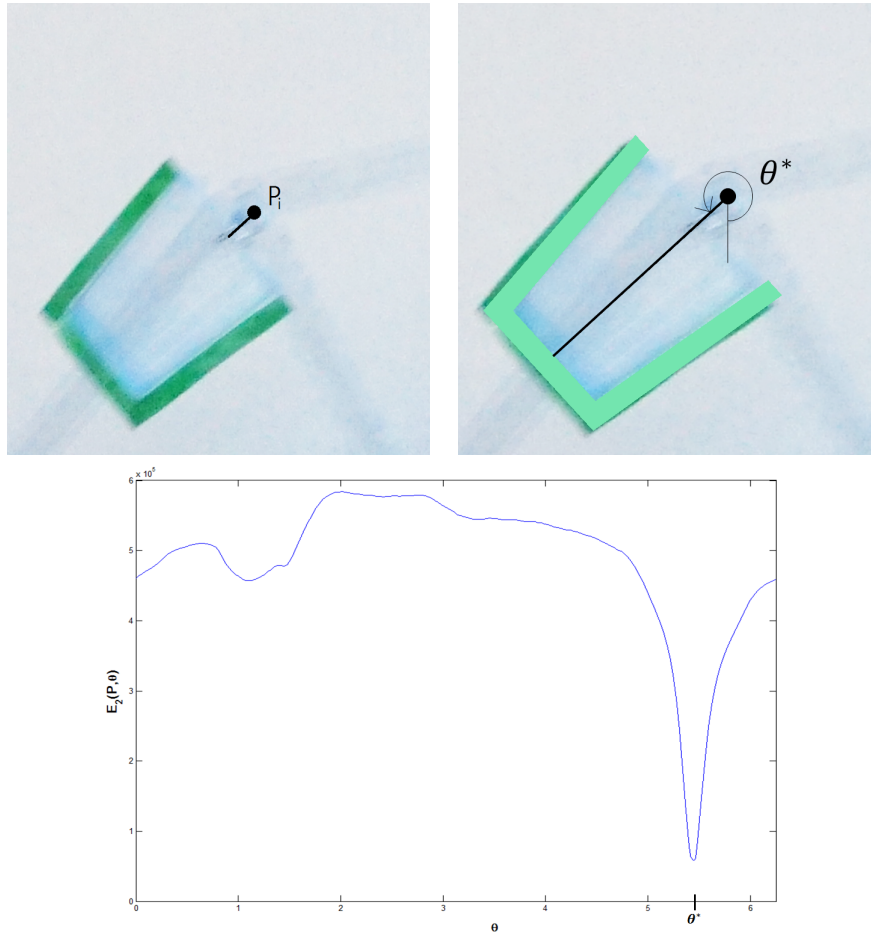


Fig. 8. Green marking tape is attached around the front section of each cup (top left). The axis of rotation in the front view is denoted by P ( top middle). The minimization point of  $E_2(P, \theta)$  (bottom) matches the actual rotation (top right).

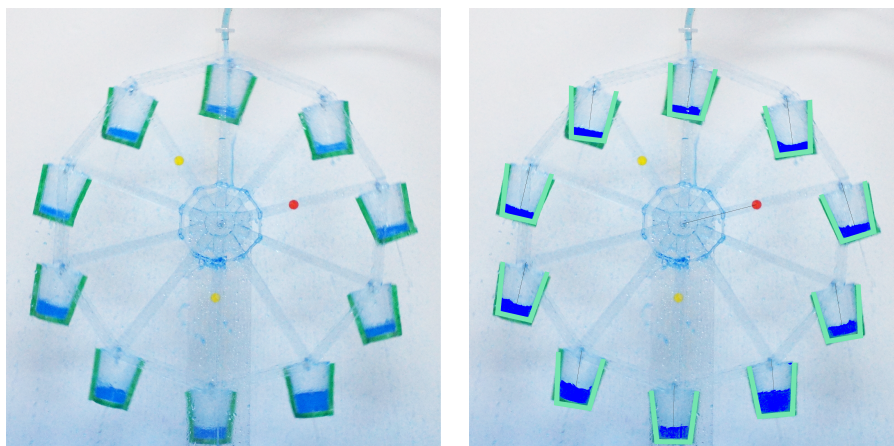


Fig. 9. Markers on the waterwheel (left) and the detected mass distribution (right)

and one value from  $(K_H, K_P)$ .

Figure 11 shows the angular velocities when  $K = K_1, K_2$ , and  $K_3$ . Since  $K_1, K_2 \in (0, K_H)$ , the bifurcation analysis states the convergence toward the stable limit cycle. A main characteristic of the limit cycle is the repetitive sign change in angular velocity. The results in the figure indicate the match between analysis and experiment: The angular velocities in the cases of  $K = K_1$  and  $K_2$  repeatedly change the sign,

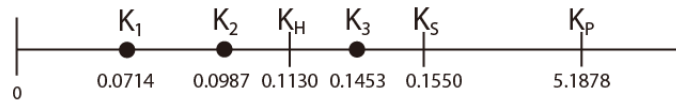


Fig. 10. We tried three  $K$  values.  $K_1 = 0.0714$ ,  $K_2 = 0.0987$ , and  $K_3 = 0.1453$ .

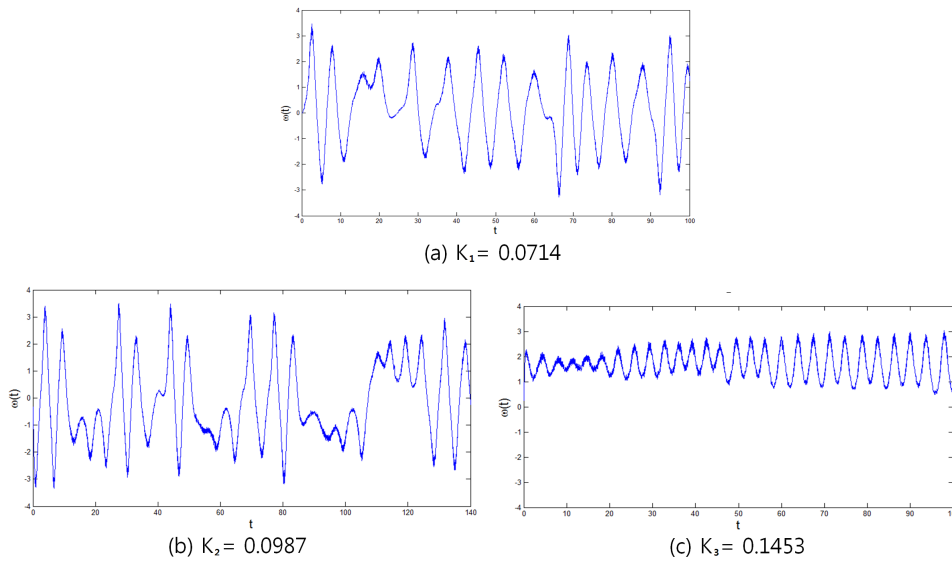


Fig. 11. Angular velocities observed when  $K = K_1$  (top),  $K_2$  (middle), and  $K_3$  (bottom).

while that of  $K = K_3$  keeps the sign.

As described in section 4, we measure not only the angular velocity  $\omega(t)$  but also the mass distribution  $m(\theta, t)$  from which  $a_1(t)$  and  $b_1(t)$  are calculated by the discrete Fourier transform [Strikwerda, 1989](page 39). Figure 12, 13, and 14 show the phase portraits of the measurements and compares them to the numerical simulations by the Runge-Kutta 4<sup>th</sup> [Iserles, 1996] for  $K = K_1, K_2$ , and  $K_3$ , respectively. The three dimensional curves from the measurements look rough and bumpy, while limit cycles from the accurate numerical simulations are smooth and clearly periodic. The roughness of the curves seems to come from a coarseness of the experimental setup and some noisy error of the measurements through the image processing. For example,

To our disappointments, the phase portraits from the measurements do not form the limit cycles from the accurate simulations: compare the top left and top right pictures in figure 12, 13, and 14. Though the noise and coarseness are present, we note that the measured phase portrait is quite similar to the union of the limit cycle and the intermediate trajectories that arise from  $C_{\pm}$  and converge toward the limit cycle, which is depicted in each bottom picture of figure 12, 13, and 14. The noise and coarseness hinders the phase portrait from the convergence to the limit cycle. The hindrance of the noise and the attraction of the limit cycle seem to make the measurement wander around the limit cycle and  $C_{\pm}$ .

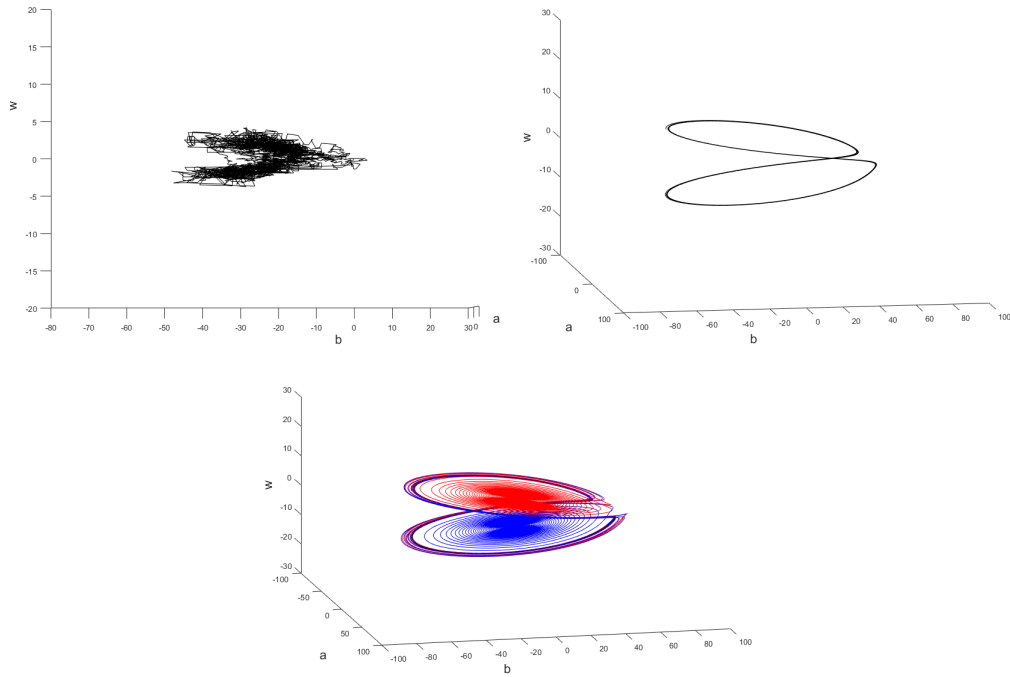


Fig. 12. Phase portraits of the measurement (top left), the numerical simulations of the limit cycle (top right) and the limit cycle with intermediate trajectories (bottom), for  $K = K_1$

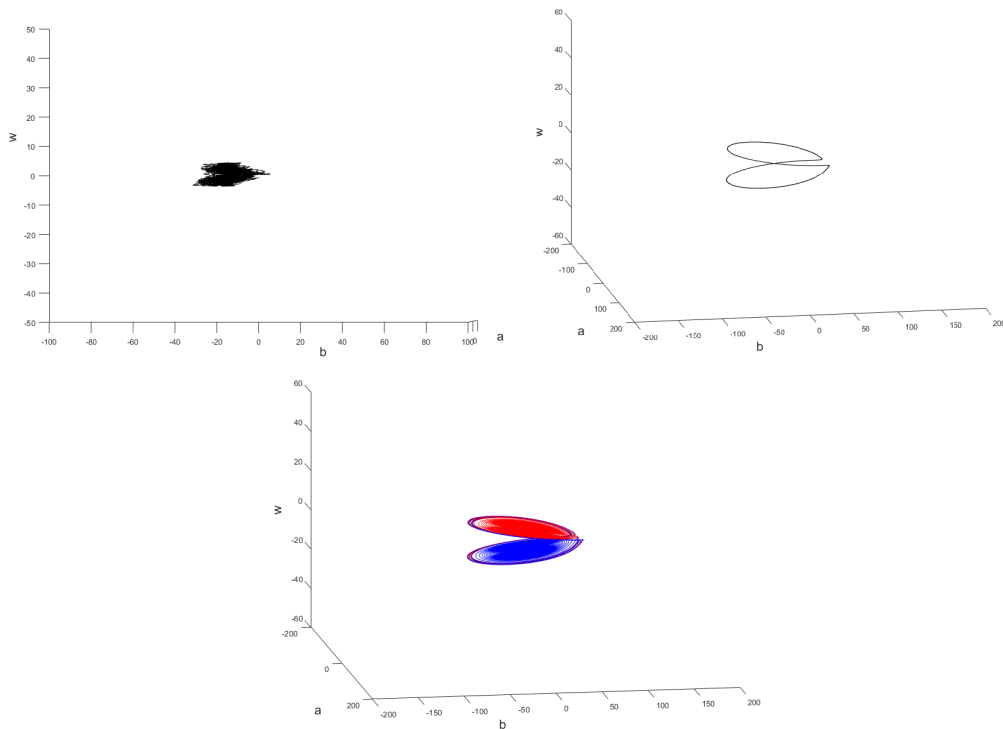


Fig. 13. Phase portraits of the measurement (top left), the numerical simulations of the limit cycle (top right) and the limit cycle with intermediate trajectories (bottom), for  $K = K_2$

## 6. Conclusion

Our experiment setup follows one of the simplest conventional setups, but achieves enhancement, through which this work is listed as one of the few experiments that record not only the angular velocity but also

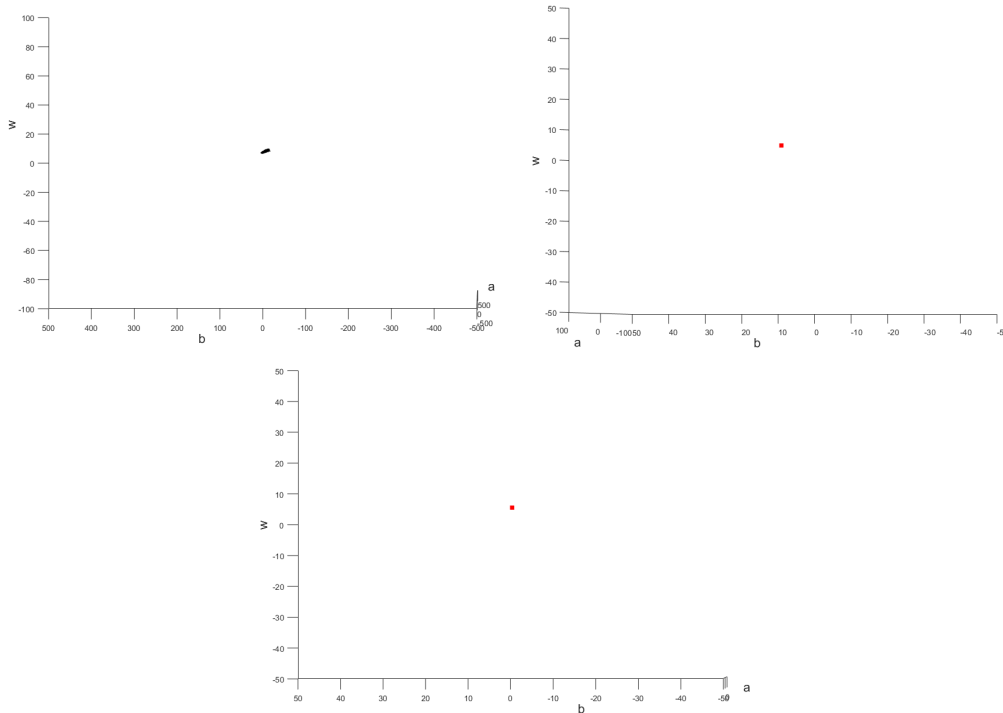


Fig. 14. Phase portraits of the measurement (top left), the numerical simulations of the limit cycle (top right) and the limit cycle with intermediate trajectories (bottom), for  $K = K_3$

the mass distribution. We built the waterwheel with transparent acrylic and used water dyed blue. The three dot markers on the middle of rims lead to the successful detection of the angle of rotation. The green marker along the section of each cup allows the rotation of the cup to be detected well. Dyed water in the cup is then easily measured.

Though our setup is simple and allows for the efficient detection of mass distribution, it suffers some errors in realizing the Lorenz equations. Because of the gaps between hanging cups, water inflow does not add up sometimes. Water leaked out of the cups in the top may flow into the cups in the below. Due to such weakness, the phase portrait from the measurement did not coincide with the limit cycle from the accurate simulation, but resembles the union of the limit cycle and the intermediate trajectories started from the fixed points. In our opinion, the experiment result does not make a complete success, but a good suggestion toward a simple and accurate experiment that measures all the state variables.

There exist more accurate experiment setups. For example, the waterwheel is located not vertically but slightly slanted. Around the wheel, long thin pipes are attached seamlessly. Although it is more accurate than our current setup, the slanted angle hinders the cups behind and the recording of the whole mass distribution requires more than two cameras with the synchronization between them. Currently, there is not a simple setup that allows for the measurement of all the state variables within our search. We put off overcoming the weakness of the current setup to future work.

## Acknowledgement

This research was supported by Basic Science Research Program through the National Research Foundation of Korea(NRF) funded by the Ministry of Education(2009-0093827).

## References

Cho, K. & Miyano, T. [2014] “Chaotic cryptography using augmented lorenz equations aided by quantum key distribution,” *IEEE Trans. Circuits Syst.* **62**, 478–487.

- Guckenheimer, J. & Holmes, P. [1983] *Nonlinear Oscillations, Dynamical Systems, and Bifurcations of Vector Fields* (Springer-Verlag, New York, NY, USA).
- Illing, L., Fordyce, R. F., Saunders, A. M. & Ormond, R. [2012] “Experiments with a malkus-lorenz water wheel: Chaos and synchronization,” *Am. J. Phys.* **80**, 192–202.
- Iserles, A. [1996] *A First Course in the Numerical Analysis of Differential Equations* (Cambridge, New York, NY, USA).
- Kolar, M. & G.Gumbs [1992] “Theory for the experimental observation of chaos in a rotating waterwheel,” *Am. Phys. Soc.* **45**, 626–637.
- Kolar, M. & Gumbs, G. [1992] “Numerical experiment of lorenz model with direct difference scheme,” *Physical Review A* **27**, 626–637.
- LaPlante, A. [2014] “How big data analytics creates order out of chaos, Nov 25th,” *Forbes Business* .
- Malkus, W. V. R. [1972] “Non-periodic convection at high and low prandtl number,” *Mem. Soc. R. Sci. Liege Collect, IV* **4**, 125–128.
- Matson, L. E. [2007] “The malkus-lorenz water wheel revisited,” *Am. J. Phys.* **75**, 1114–1122.
- Mishra, A. A. & Sanghi, S. [2006] “A study of the asymmetric malkus waterwheel: The biased Lorenz equations,” *Chaos* **16**, 013114.
- Nemirovsky, R. [1993] “Students making sense of chaotic behavior,” *Interactive Learning Environments* **3**, 151–175.
- Perko, L. [2001] *Differential Equations and Dynamical Systems*, 3rd ed. (Springer-Verlag, New York, NY, USA).
- Strikwerda, J. C. [1989] *Finite Difference Schemes and Partial Differential Equations*, 2nd ed. (Chapman & Hall, Philadelphia, PA, USA).
- Strogatz, S. H. [2008] *Nonlinear Dynamics and Chaos: With Applications to Physics, Biology, Chemistry, and Engineering* (Westview Press, Cambridge, MA, USA).
- Tongen, A., Thelwell, R. & Becerra-Alonso, D. [2012] “Reinventing the wheel: The chaotic sandwheel,” *Am. J. Phys.* **81**, 127–133.
- Yang, S. & Lin, Y. [1998] “Numerical experiment of lorenz model with direct difference scheme,” *Kybernetes* **27**, 674–690.